

Point Sources from Dissipative Dark Matter

Prateek Agrawal and Lisa Randall

Department of Physics, Harvard University, Cambridge, MA 02138, USA

ABSTRACT: If a component of dark matter has dissipative interactions, it can cool to form compact astrophysical objects with higher density than that of conventional cold dark matter (sub)haloes. Dark matter annihilations might then appear as point sources, leading to novel morphology for indirect detection. We explore dissipative models where interaction with the Standard Model might provide visible signals, and show how such objects might give rise to the observed excess in gamma rays arising from the galactic center.

Contents

1	Introduction	1
2	Compact objects from dissipative dark matter	2
2.1	Dark Disk Fragmentation and the size of clouds	3
3	Dissipative Dark Matter Models	5
3.1	A simple dissipative dark matter model	5
3.2	Portal Models	5
3.2.1	A massless Z' portal	6
3.2.2	A massive Z' portal	8
4	Phenomenology	9
4.1	Relic abundance	9
4.2	Cooling	11
4.3	Direct detection	13
4.4	Constraints on compact objects	14
5	The Galactic Center Excess	15
5.1	Spectrum for the Galactic Center excess	16
5.2	The Point-like GeV Excess from Compact Objects in Dissipative Dark Matter	17
6	Conclusion	18

1 Introduction

A vast amount of astrophysical evidence exists for the presence of dark matter, but its particle physics nature remains entirely unknown. Various direct and indirect detection experiments that search for small non-gravitational interactions between the dark and Standard Model sectors hope to find this dark component of our energy density.

If the Standard Model (SM) is a guide, the dark sector may contain multiple species, with small components possessing stronger interactions, amongst itself and/or with the SM. Even if this component is subdominant – so that it does not impact gravitational measurements of dark matter so far – it might generate the first signals we discover.

One such class of models is where such a dark matter fraction has dissipative dynamics [1, 2]. In analogy with baryonic matter, this could lead to the formation of interesting astrophysical structures, without disrupting qualitative features of cold dark matter halo formation. If this component also interacts non-gravitationally with the Standard Model, the first signals of dark matter might have unexpected properties [3–12].

In this paper, we consider the possibility that dark matter forms dense clouds that are sites of enhanced annihilation. These novel astrophysical structures – such as a dark disk or dense compact halo objects – will give rise to distinctive morphology for indirect detection. If small enough, these

clouds would appear as point sources in indirect detection experiments. We explore models with both dissipative interactions and couplings to the SM that can give rise to visible signatures from dark compact objects, with the specific signal depending on the particular nature of this coupling. We will see that one of the most interesting aspects of such models is that the dissipative dark matter can be a negligible fraction of the total dark matter composition, yet still give rise to observable effects.

An important signal is the excess of gamma rays observed from towards the galactic center [13–17], with some statistical evidence supporting this excess as arising from point sources [18–20], though this may be due to substructure in background that is not modeled in the range of diffuse background models considered (see also [21]). The more conventional assumption for sources that would produce the observed point-like spectrum could be a new population of millisecond pulsars (MSPs), with luminosity just below the Fermi point source detection threshold. Direct evidence for such a population has not yet been observed (see also [20, 22, 23]). If we are to definitely establish the origin, it is worthwhile to consider less conventional potential sources as well. An alternative admittedly more speculative possibility that is also worth investigating is that the excess is associated with dark point sources. In this paper we consider pointlike sources that arise from dissipative dynamics in the dark sector. In this scenario the dark objects cool analogous to the objects in the SM sector. In our case we only have a $U(1)$ interaction that leads to cooling, and we study the compact objects that would result from this interaction. An alternative is ultra-compact minihaloes (UCMHs) [24–33] and we discuss ways to distinguish them at the end.

This paper is organized as follows. We start in section 2 explaining how dissipative dark matter can give rise to compact objects and present a model-dependent estimate for their expected sizes. In section 3 we introduce a simple dissipative dark matter model and specific portal couplings to the Standard Model. We analyze the resulting phenomenology in section 4. Section 5 shows how such a model could account for the Galactic Center excess, and we conclude in section 6.

2 Compact objects from dissipative dark matter

If there is a component of dark matter that has dissipative dynamics, it can cool efficiently with the potential creation of compact objects. The sizes and distribution of such objects depends on nonlinear dynamics, and a careful prediction would require modeling and simulations. However, simple estimates demonstrate that compact objects, with size determined by fraction of dark matter in the charged dark component, are a viable possibility.

We assume the dissipative component leads to formation of an unstable disk which then fragments via Toomre instabilities to form compact objects. An alternative possibility is that compact objects form in smaller subhaloes and might survive as subhaloes merge to form our galaxy. This latter scenario could potentially lead to compact objects with a distribution different from the one we now consider but is worth independent consideration.

When formed from disk fragmentation, the typical size of the objects can be estimated using a simple stability analysis, which we perform below. For simplicity, we assume that the clumps are uniform so that we can characterize parameterize the distribution and mass functions with a single characteristic size and mass, $\{M, R\}$, dictated by the stability analysis. More generally, one could parameterize the number of objects of mass M by the mass function, dN/dM and assume a nonuniform density even within the objects.

We will consider a simple dissipative model with a weak-scale particle X and a light particle C , both charged under a dark $U(1)$ with coupling strength α_D . This model is discussed in further detail in section 3.

2.1 Dark Disk Fragmentation and the size of clouds

The stability condition for the dark disk in the presence of various gas and stellar components can be written using the dispersion relation for a density perturbation [8, 34–37],

$$2\pi Gk \sum_{\text{collisional}} \frac{\Sigma_i}{\kappa^2 + k^2 c_i^2 - \omega^2} + 2\pi Gk \sum_{\text{collisionless}} \frac{\Sigma_i \mathcal{F}(\omega/\kappa, k^2 \sigma_i^2/\kappa^2)}{\kappa^2 - \omega^2} = 1 \quad (2.1)$$

The gas and the dissipative component of dark matter are collisional, while the various population of stars are collisionless. The epicyclic frequency $\kappa = 36 \text{ km s}^{-1} \text{ kpc}^{-1}$, and k denotes the wavenumber of the perturbation. Σ_i is the column density of component i , and $c_i(\sigma_i)$ is the sound speed (velocity dispersion) of the collisional (collisionless) component. The function \mathcal{F} is

$$\mathcal{F}(s, \chi) = \frac{2(1-s^2)e^{-\chi}}{\chi} \sum_{n=1}^{\infty} \frac{I_n(\chi)}{1-s^2/n^2}. \quad (2.2)$$

I_n is the Bessel function of order n . The perturbation is unstable when $\omega^2 < 0$. Since the l.h.s in equation 2.1 is a monotonically increasing function of ω when $\omega < \kappa$, the instability criteria can be restated as the condition that the l.h.s is greater than 1 at $\omega = 0$,

$$2\pi Gk \sum_{\text{collisional}} \frac{\Sigma_i}{\kappa^2 + k^2 c_i^2} + 2\pi Gk \sum_{\text{collisionless}} \frac{\Sigma_i \mathcal{F}(0, k^2 \sigma_i^2/\kappa^2)}{\kappa^2} > 1. \quad (2.3)$$

The sound speed for the dark disk can be estimated by the temperature dissipative dark matter cools down to, which is roughly the temperature at which recombination occurs and rapid cooling ceases: $T \sim \frac{1}{40} m_C \alpha_D^2$,

$$c_{XC} \sim \frac{\alpha_D}{\sqrt{40}} \sqrt{\frac{m_C}{m_X}} \quad (2.4)$$

We show the stability condition in figure 1. Note that in the Milky Way, galaxy stars and gas are relevant to stability only on larger length scales. For our choice of parameters, the dark disk induces instability at much shorter length scales, where the contribution of stars and gas to the dispersion relation can be neglected. It therefore suffices here to consider the stability of the dark disk by itself and find a simple expression for the wavenumber of unstable modes $k_- < k < k_+$,

$$k_{\pm} = \frac{\pi G \Sigma_{XC}}{c_{XC}^2} \pm \sqrt{\left(\frac{\pi G \Sigma_{XC}}{c_{XC}^2}\right)^2 - \frac{\kappa^2}{c_{XC}^2}}. \quad (2.5)$$

The fastest growing mode corresponds to $k = \pi G \Sigma_{XC} / c_{XC}^2$.

We assume the dark disk surface density is

$$\Sigma_{XC}(r) = \Sigma_{XC,\odot} e^{-(r-r_{\odot})/r_d} \quad (2.6)$$

where $r_d \simeq 3 \text{ kpc}$ is the assumed scale radius of the dark disk, and $\Sigma_{XC,\odot}$ is the local dark disk surface density which can be as large as $\sim 10 M_{\odot} / \text{pc}^2$ [11]. Therefore the wavenumber varies as a function of distance from the center since the density and hence the stability criterion vary.

The dark compact objects that will be formed then have mass approximately $M = \pi \Sigma_{XC} \mathcal{R}_{T_{oomre}}^2$, where $\mathcal{R}_{T_{oomre}}$ is the wavelength of the fastest growing mode. In figure 2 we show the size and mass of this mode as a function of the distance from the Galactic Center. We see that in this scenario

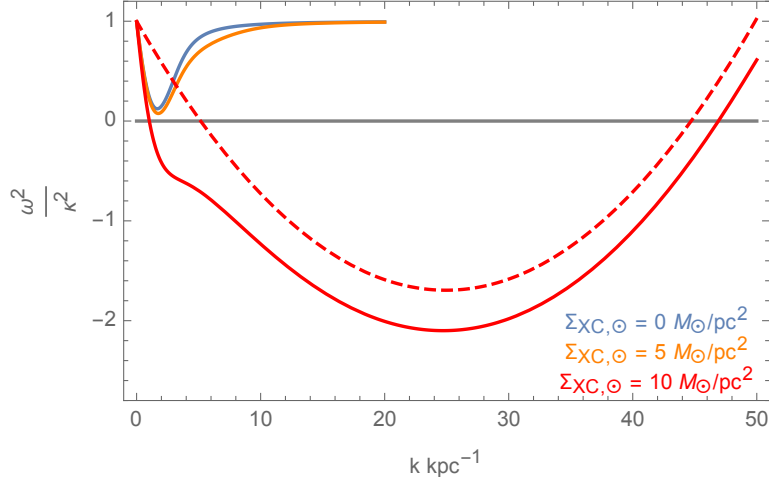


Figure 1: Instability ($\omega^2 < 0$) in the galactic disk at the solar system as a function of the wavenumber of the perturbation for different column densities of the dark disk. We also show the instability curve obtained by considering the dark disk in isolation (dashed). The XC dark matter sound speed was taken as 2.5 km/s (corresponding to $\alpha_D = 0.01$, $m_C = 0.2$ MeV, $m_X = 25$ GeV). Values for star and gas components were taken from McKee et al [38].

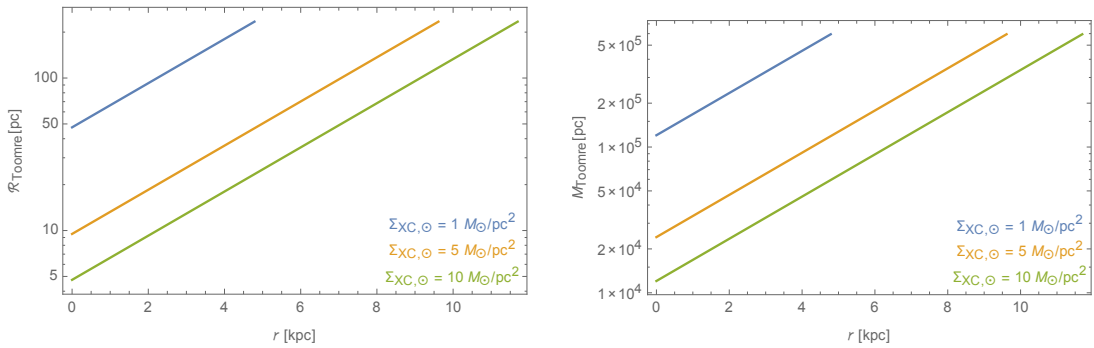


Figure 2: The initial size and mass of the fastest growing Toomre instability as a function of distance from the Galactic Center. The parameters here are $\alpha_D = 0.01$, $m_C = 0.2$ MeV, $m_X = 25$ GeV, and $r_d = 3$ kpc.

we expect objects of mass $10^4 M_\odot$, with a radius ~ 10 pc in the inner part of the galaxy. Of course, this is a very crude estimate of the initial size, and this object might undergo further collapse, tidal disruption, evaporation or accretion.

We note that the spatial distribution of the objects would require more detailed simulations. Clumps might be dominantly clustered in the inner galaxy, spread through the disk, or distributed throughout the dark matter halo. We will assume that the dark matter also forms a disk + bulge system, with the disk subject to fragmentation. By analogy with the bulge, this would lead to a population of dark compact objects at the center of the galaxy in a roughly spherical distribution. In principle compact objects can form throughout the bulk as well, though the answer would depend on whether such objects fall to the center and shock heating repeats itself. For now we assume compact

objects are concentrated in the center and the disk, and ask what the consequences for indirect detection might be. We will focus on the objects in the inner galaxy, and not consider other potential visible signals from the plane of the disk or the halo which would require detailed simulations.

3 Dissipative Dark Matter Models

Dark matter with dissipative dynamics was considered in Ref. [1, 2]. In this section we expand the discussion to include the possibility that in addition to dissipative self-interactions there are also interactions with the Standard Model. In this case we can have dissipative interactions that lead to the formation of compact objects and these in turn can potentially give rise to visible signatures.

3.1 A simple dissipative dark matter model

The model consists of a heavy dark proton X and a lighter dark electron C , both charged under a dark U(1) gauge group, as in [1, 2, 39].

$$\mathcal{L} = -\frac{1}{4}V_{\mu\nu}V^{\mu\nu} + eJ_{EM}^\mu A_\mu + gV_\mu (\bar{X}\gamma^\mu X + \bar{C}\gamma^\mu C) \quad (3.1)$$

A sufficiently large relic population of a light enough C would lead to efficient cooling in dark matter haloes. Being light, C s would annihilate efficiently, and survive only if produced through non-thermal processes – such as a matter-antimatter asymmetry in the population. We consider models in which there is both a symmetric relic abundance of X and \bar{X} particles, as well as an asymmetric population of C and X . Such a symmetric population would occur naturally for dark matter masses comparable to the weak scale, just as for the more usual WIMPs. By charge neutrality $n_C - n_X + n_{\bar{X}} = 0$. We define the fraction of XC dark matter in the asymmetric component by

$$f_{(XC)} \equiv \frac{\rho_C + \rho_X - \rho_{\bar{X}}}{\rho_C + \rho_X + \rho_{\bar{X}}} \approx \frac{n_X - n_{\bar{X}}}{n_X + n_{\bar{X}}} \quad (3.2)$$

We also define the fraction of dark matter density in the charged system,

$$f = \frac{\Omega_X}{\Omega_{DM}} \quad (3.3)$$

with Ω_X the energy total density in X, \bar{X} and C . The rest of the dark matter is assumed to be made up of a distinct cold dark matter (CDM) component.

To generate visible indirect signatures, the model must also include “portal” interactions with the SM. A simple option is a kinetic mixing portal, in which the dark photon kinetically mixes with the SM photon. However, constraints on millicharged particles coupled with constraints on the survival of the compact objects necessitate an additional dark gauge Z' , which can be either massless or massive—resulting in different signatures that we outline below.

3.2 Portal Models

We first pursue the simplest possibility for interactions between the dark and Standard Model sectors and see why that is not so promising for current indirect detection measurements. Dark matter can interact with the SM through kinetic mixing of the dark photon with the SM photon [40, 41],

$$\mathcal{L} = -\frac{\epsilon}{2} \frac{e}{g_D} F_{\mu\nu} V^{\mu\nu} . \quad (3.4)$$

When the dark photon mass is zero, it is convenient to redefine the dark photon

$$V_\mu \rightarrow V_\mu - \epsilon \frac{e}{g_D} A_\mu \quad (3.5)$$

After rescaling V to obtain a canonical kinetic term, this yields the Lagrangian (to leading order in ϵ)

$$\mathcal{L} = -\frac{1}{4} F_{\mu\nu} F^{\mu\nu} - \frac{1}{4} V_{\mu\nu} V^{\mu\nu} + e J_{EM}^\mu A_\mu + g_D V_\mu (\bar{X} \gamma^\mu X + \bar{C} \gamma^\mu C) + e \epsilon A_\mu (\bar{X} \gamma^\mu X + \bar{C} \gamma^\mu C) \quad (3.6)$$

There is no direct coupling of V to matter in this basis, but the dark matter particles pick up a millicharge $e\epsilon$ under the SM photon [41].

Models with millicharged particles (MCPs) have rich phenomenology, and the millicharge has many constraints depending on the mass of the particle [42–55]. We summarize the constraints in figure 3.

For very light particles, $m_C < 10$ keV, star cooling constraints restrict $\epsilon < 10^{-14}$ [50, 51]. In the range of C masses where cooling occurs efficiently, $m_C \sim$ MeV, very stringent bounds on ϵ are needed to prevent dark photons from contributing $N_{\text{eff}} \sim 1$ to the cosmic microwave background (CMB) and during Big Bang nucleosynthesis (BBN) [48, 50]. The bound relies on thermal coupling and corresponds to when the sectors thermally decouple. The dark sector is coupled to the photon bath through the process $e^+ e^- \rightarrow C \bar{C}$. The rate for this process relative to Hubble is,

$$\frac{n_e \langle \sigma v \rangle}{H} \sim \frac{g T^3}{\pi^2} \frac{\pi \alpha^2 \epsilon^2}{T^2} \frac{M_{pl}}{T^2} \quad (3.7)$$

Thus, the condition that the dark sector not get into thermal contact with the SM at temperature $T = m_C$,

$$\epsilon \lesssim \left(\frac{m_C}{\alpha^2 M_{pl}} \right)^{\frac{1}{2}} \sim 10^{-9} \left(\frac{m_C}{1 \text{ MeV}} \right)^{\frac{1}{2}} \quad (3.8)$$

This is an extremely severe bound and forces ϵ to be too small to produce observable indirect detection signals. Interesting signals arise only in the presence of additional interactions, as we now propose.

3.2.1 A massless Z' portal

	$U(1)_D$	$U(1)_{Z'}$
X	1	1
X^c	-1	-1
C	-1	0
C^c	1	0
Y	-1	1
Y^c	1	-1

(3.9)

Table 1: Particle content for the massless Z' portal model.

The kinetic mixing of the dark photon with the SM photon leads to a millicharge for the light particle C , which is also severely constrained. However, an additional massless gauge boson, Z' , which

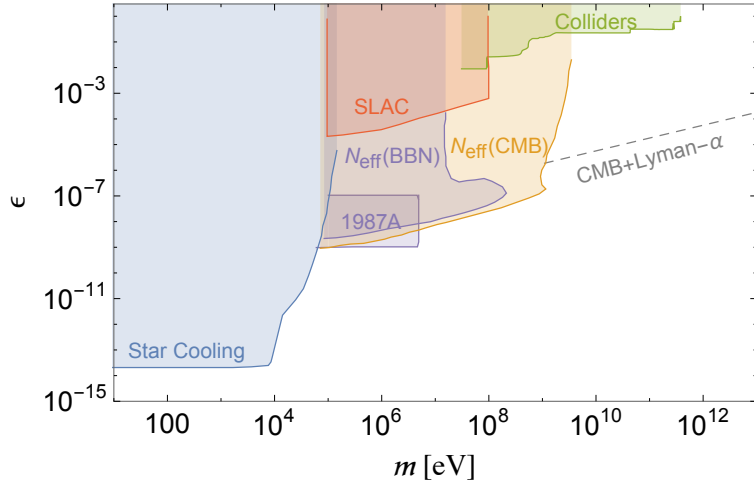


Figure 3: Constraints on millicharged particles from star and supernova cooling [50, 51], N_{eff} during BBN and CMB [48, 50], collider experiments [42, 43, 56, 57]. The gray dashed line shows the constraint from CMB anisotropy and Lyman- α measurements [44, 47, 49] assuming that the MCP makes up all of the dark matter.

couples to X but not to C , can have a moderate kinetic mixing with the hypercharge gauge boson and produce observable signals at direct and indirect detection experiments, or at colliders.

As an example, we consider a model with 3 $U(1)$ gauge symmetries – hypercharge $U(1)_Y$, the dark photon $U(1)_D$ and the Z' portal $U(1)_{Z'}$. The SM particles are not charged under the $U(1)_D$ or the $U(1)_{Z'}$, and the dark sector particles are not charged under the SM gauge group. We assume that there is no kinetic mixing between the $U(1)_D$ and either $U(1)$, only between $U(1)_{Z'}$ and $U(1)_Y$,

$$\mathcal{L} = -\frac{\epsilon}{2} \frac{e}{g_{Z'}} Z'_{\mu\nu} F^{\mu\nu} \quad (3.10)$$

We summarize the particle content of the model in table 1. The presence of only vectorlike fermions beyond the SM ensures that there are no anomalies. If we want to have a cosmological population of XC atoms (which have a net charge under the $U(1)_{Z'}$), we need a corresponding population of Y particles to ensure that the universe is charge neutral under $U(1)_{Z'}$. We note that for this particular choice of charges, there is no kinetic mixing induced by X, Y, C loops between the $U(1)_D$ and the $U(1)_{Z'}$. For simplicity we assume below that the Y particle has roughly the same mass as X , $m_Y \sim m_X$.

The dominant constraints on this scenario come from cosmological and astrophysical observations (for proposals to cover this parameter space in collider experiments see [58, 59]). There are bounds on this scenario from CMB and Lyman- α measurements [45, 47, 49]. The bound on kinetic mixing assuming X makes up all of dark matter is

$$\epsilon \lesssim 1.8 \times 10^{-6} \left(\frac{m_X}{\text{GeV}} \right)^{1/2} \quad (3.11)$$

in order for X s to be kinetically decoupled from baryons during recombination. For larger values of the mixing, X and Y can only make up small fraction, of the total dark matter [47], $\Omega_X < 0.001$ (where Ω_X is the energy density of the free X, Y particles). There are also potentially strong constraints

($\epsilon \lesssim 10^{-14}(m_X/\text{GeV})$) from the measurement of shapes of cluster haloes, which would be affected due to the cluster magnetic force on the MCP dark matter [54]. However, this constraint is likely to be dramatically weakened if the MCP makes up only a fraction of the dark matter density.

A promising signal in this model arises from the annihilation of dark matter to SM photons through X millicharge [60]. The annihilation cross section for $X\bar{X} \rightarrow \gamma Z', \gamma \gamma_D$ is,

$$\langle\sigma v\rangle_{X\bar{X}\rightarrow\gamma Z'/\gamma_D} = \frac{\pi\epsilon^2\alpha(\alpha_{Z'} + \alpha_D)}{m_X^2} \quad (3.12)$$

There is also continuum gamma-ray emission originating from $X\bar{X}$ annihilations to SM fermions through an s -channel photon. However, for comparable mass and couplings, as is expected in a dissipative scenario, the relative rate of the line emission and continuum emission are comparable:

$$\frac{\langle\sigma v\rangle_{X\bar{X}\rightarrow\gamma Z'/\gamma_D}}{\langle\sigma v\rangle_{X\bar{X}\rightarrow f\bar{f}}} = \frac{\alpha_{Z'} + \alpha_D}{\alpha} \quad (3.13)$$

The FERMI sensitivity for the line signal [61] is about 3 orders of magnitude stronger than the continuum emission sensitivity. This implies that for $\alpha_{Z'} + \alpha_D > 10^{-5}$, the line constitutes a more promising avenue for detection of this model.

A search for a line spectrum from a point source will be interesting to carry out since it has the cleanest spectrum and morphology in indirect searches. A spectral analysis of unassociated point sources will be relatively simple, but a stacked analysis or a statistical analysis along the lines of [18, 62] would likely have a higher sensitivity. Note that even in presence of a small mixing as in equation 3.11, it can be possible to get an observable signal from point sources.

3.2.2 A massive Z' portal

We now consider a massive Z' , which in some respects most closely mimics the gauge structure in the Standard Model. In this case the dominant signal is continuum photons. As above, C does not couple to Z' . In this case, we do not require the presence of the additional fermion Y . This model is similar in some respects to that considered in [63].

We can write the leading interactions of the Z' as,

$$\mathcal{L} = -\frac{\epsilon}{2}Z'_{\mu\nu}F^{\mu\nu} + Z'_\mu g_Z \bar{X}\gamma^\mu X + m_{Z'}^2 Z'_\mu Z'^\mu \quad (3.14)$$

We work in the basis where only the visible matter coupling to the Z' boson is through kinetic mixing, and the dark matter does not pick up any charge under the usual photon. This interaction can produce signals at direct or indirect detection experiments, as well as collider signals. Our focus is the indirect detection signal of an excess in gamma rays from the Galactic Center. In that respect, the annihilation to Z' pairs mimics the annihilation to the b -quarks in the models of Ref. [15, 64–66], which is seen to give a good fit.

We show the collider limits on the massive Z' portal in figure 4 (also see [85] for a detailed review of constraints and future prospects, and for further references). A number of future experiments/analyses aim to cover new parameter space for this model [86–92]. In the next section we study in detail the phenomenology of dissipative dark matter with the massive Z' portal. This model can potentially explain the excess gamma ray photons observed from the galactic center, which we return to in section 5.

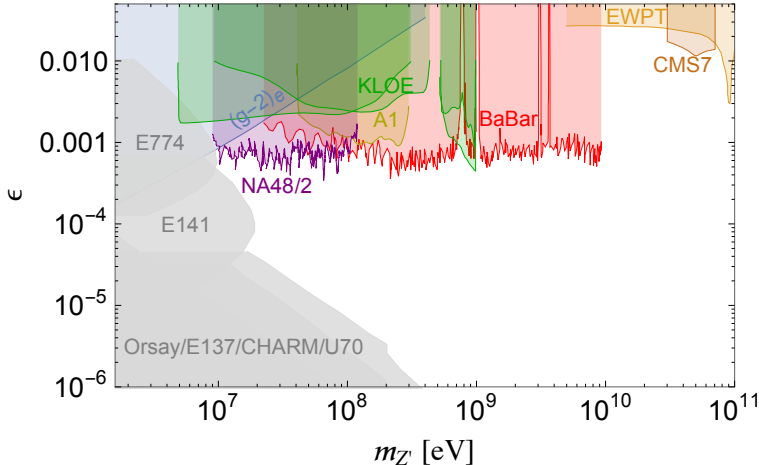


Figure 4: Constraints on the kinetic mixing parameter for a massive Z' portal as a function of the Z' mass. The constraints shown are from beam-dumps [67–71], supernovae [72, 73], BaBar [74], A1 [75], KLOE [76–79], anomalous magnetic moment of the electron [80, 81], the NA48/2 experiment at CERN [82], electroweak precision measurements [83] and Drell-Yan production at the LHC [84].

4 Phenomenology

4.1 Relic abundance

A crucial ingredient for dissipative dynamics is the presence of the light C particles. This requires an asymmetry in C , since the symmetric population annihilates efficiently. On the other hand, the indirect detection signal from $X\bar{X}$ annihilation requires a symmetric component to survive as well. Thus, we are led to consider a freezeout where both a symmetric as well as an asymmetric component survives.

An alternative where the halo also consisted of charged dark matter was considered in [12, 93]. Here we restrict to the possibility that only a fraction of the total dark matter is in X, \bar{X}, C particles.

A detailed calculation of the relic abundance in a very similar model was presented in [12] (see also [94–96]), so here we just recall the important results. The key differences from the standard relic abundance calculation are the presence of an asymmetric component and a relative temperature between the dark and SM sectors, $\xi = T_D/T$. If the interactions between X and the SM are small, the dominant annihilation channels for X will be in the dark sector, $\gamma_D\gamma_D/Z'Z'/\gamma_D Z', C\bar{C}$. We define the ratio of the population of \bar{X} and X as r ,

$$r = \frac{Y_{\bar{X}}}{Y_X} \quad (4.1)$$

such that the value of the ratio today, r_∞ , characterizes how much of the symmetric and asymmetric components survive. We define the asymmetry,

$$\eta = Y_X - Y_{\bar{X}} = Y_C - Y_{\bar{C}}. \quad (4.2)$$

η is a constant that is set at early times, and we treat it as a free input parameter.

The Boltzmann equation in terms of r and $x = m_X/T$ is,

$$\frac{dr}{dx} = -\frac{\lambda(x)\eta}{x^2} \left[r - r_{eq}(x) \left(\frac{1-r}{1-r_{eq}(x)} \right)^2 \right] \quad (4.3)$$

We have defined λ and r_{eq} ,

$$\lambda(x) = \sqrt{\frac{\pi}{45G_N}} g_*^{1/2} m_X \langle \sigma v \rangle \quad (4.4)$$

$$r_{eq}(x) = \frac{Y_{\bar{X}}^{eq}}{Y_X^{eq}} = \exp \left(-2 \sinh^{-1} \frac{\eta}{2Y_{eq}(x)} \right) \quad (4.5)$$

$$Y_{eq}(x) = \sqrt{Y_X^{eq} Y_{\bar{X}}^{eq}} \simeq \frac{45g_X}{4\sqrt{2}\pi^{7/2} h_{eff}(x)} x^{3/2} \xi^{3/2} e^{-x/\xi} \quad (4.6)$$

The values for $g_*^{1/2}$, h_{eff} are tabulated in [97], and $g_X = 2$ is the number of degrees of freedom of X, \bar{X} . $\lambda(x)$ is roughly constant, since the annihilation cross section is

$$\langle \sigma v \rangle_{ann} = \frac{\pi\alpha_D^2}{m_X^2} + \frac{\pi(\alpha_D + \alpha_{Z'})^2}{m_X^2} \equiv \frac{\pi\alpha_{eff}^2}{m_X^2} \quad (4.7)$$

to leading order in $m_{Z'}/m_X$ (for the couplings we are interested in, the Sommerfeld enhancement during thermal freezeout is negligible).

We use an approximation for r_∞ by integrating the Boltzmann equation from the freeze-out temperature x_f to today neglecting r_{eq} , and with the boundary condition $r(x_f) = r_{eq}(x_f)$. The value x_f can be found by solving the following implicit equation,

$$\frac{dr_{eq}(x_f)}{dx} = -\frac{\lambda(x_f)\eta}{x_f^2} r_{eq}(x_f) \quad (4.8)$$

with the approximate solution,

$$x_f \simeq \xi_f \left[\log \left(\xi_f^{3/2} \lambda \frac{45g_X}{4\sqrt{2}\pi^{7/2} h_{eff}(x_f)} \right) - \frac{1}{2} \log(x_f) + \log \left(1 + \frac{1}{6} \left(\frac{\eta\lambda}{2x_f^2} \right)^2 \right) \right]. \quad (4.9)$$

The value of r_∞ obtained through this procedure is a good approximation to the numerical solution.

$$r_\infty \simeq r_{eq}(x_f) \exp \left(-\frac{\lambda(x_f)\eta}{x_f} \right) \quad (4.10)$$

Note that λ is directly related to the relic abundance in the limit $\eta \rightarrow 0$ (i.e. in the absence of an asymmetry),

$$Y_\infty^{\eta=0} \simeq \frac{x_f}{\lambda(x_f)}, \quad (4.11)$$

so that,

$$r_\infty \simeq r_{eq}(x_f) \exp \left(-\frac{\eta}{Y_\infty^{\eta=0}} \right) \quad (4.12)$$

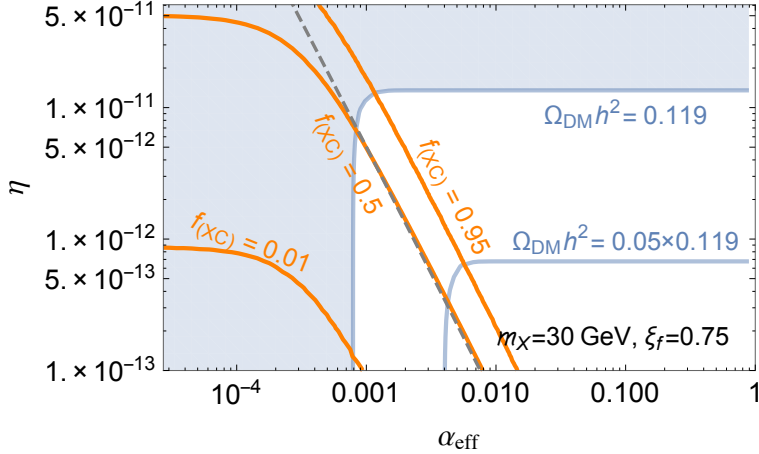


Figure 5: The relic abundance for the XC component of dark matter. The effective coupling α_{eff} is defined in equation 4.7. The blue lines are contours of $\Omega_X h^2$ and the orange lines are contours of $f_{(XC)}$. The gray dashed line shows the turn-over point where $\eta = Y_\infty^{\eta=0}$. We chose $m_X = 30$ GeV for this plot with $\xi_f = 0.75$.

For the parameter space of interest to us, $r_{\text{eq}}(x_f) \simeq 1$. The dark matter density today is

$$\Omega_X h^2 = \frac{\Omega_B h^2}{\eta_B} \frac{m_X}{m_p} (Y_X(x_0) + Y_{\bar{X}}(x_0)) = \Omega_B h^2 \frac{\eta}{\eta_B} \frac{m_X}{m_p} \frac{1 + r_\infty}{1 - r_\infty} \quad (4.13)$$

where Ω_B, η_B are the baryonic energy density and asymmetry respectively, and x_0 is the value of x today.

In figure 5 we show the region of $\alpha_{\text{eff}}-\eta$ parameter space where a significant symmetric dark matter relic abundance survives in the presence of an asymmetry. The blue curves are contours of constant dark matter relic density Ω_X , and the orange lines denote the value of $f_{(XC)}$, defined in equation 3.2. The shaded region is excluded in this model as too much dark matter would survive.

We see that there are two limiting behaviors of the solutions. When $\eta \ll Y_\infty^{\eta=0}$, the result is essentially the symmetric freezeout value. Conversely, for $\eta > Y_\infty^{\eta=0}$, the relic abundance is mainly set by the asymmetry. For appreciable amounts of both symmetric and asymmetric components, we choose parameters in the turnaround region, $\eta \sim Y_\infty^{\eta=0}$.

4.2 Cooling

We now consider how dark matter haloes might cool through dissipation to form compact objects with enhanced density. The cooling calculation and requisite parameter space follows closely the one outlined in [1], with the modification due to additional \bar{X} particles [12].

The dissipative component of dark matter behaves in analogy to baryonic matter during galaxy formation. Clumps of X, C, \bar{X} accrete onto the CDM halo, and are subsequently shock heated to its virial temperature. If this temperature is larger than the binding energy of the XC bound state, then the charged X and C can radiate. The lighter C dominates the cooling and leads to collapse into a region with lower velocity than that in the dark matter halo and can in principle form a disk. The cooling time of dissipative dark matter must be smaller than the age of the universe (more precisely the dynamical time of the virialized halo) for disks or compact structures to form.

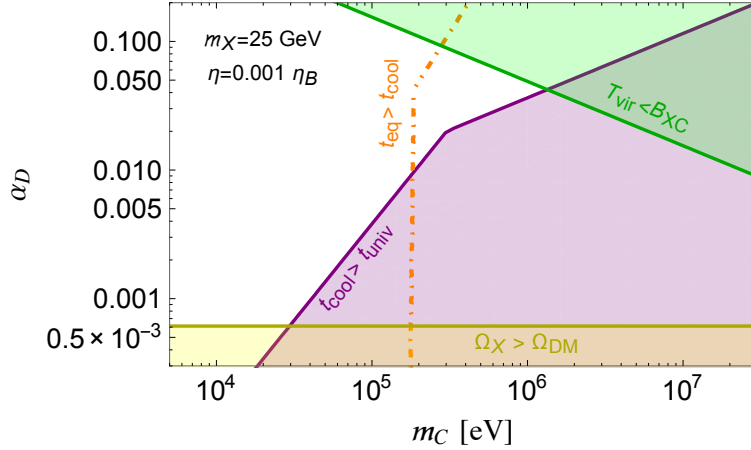


Figure 6: Constraints on the XC model in the m_C - α_D plane. Shown are constraints from relic abundance (yellow), reionization in galaxies (green), cooling rate (purple), and region where the XC particles are in thermal equilibrium (orange dot-dashed). We have ignored the contribution of $\alpha_{Z'}$ to the relic abundance for this plot.

The subsequent behavior of the dark matter gas depends on the nature of the collapse and other details of the model. For baryonic matter this collapse leads to sites of star formation. In principle high density compact objects can result from this collapse in the dark sector as well, though in the absence of additional forces one would not expect nuclear burning or feedback.

We assume the initial condition of a shock heated gas inside a CDM halo of mass $M_{gal} \simeq 10^{12} M_\odot$ and virial radius $R_{vir} \simeq 110$ kpc. We estimate the cooling timescale for the scenario where the XC dark matter initially falls into the CDM halo with a Navarro-Frenk-White (NFW) profile with a scale radius $R_s = 20$ kpc. The virial temperature for this case is

$$T_{vir} = \frac{G_N M_s \mu}{5 R_s}, \quad (4.14)$$

where $\mu = m_X / (1 + f_{(XC)})$ is the average mass of a particle in the dark matter gas, and $M_s \simeq 2 \times 10^{11} M_\odot$ is total halo mass inside the scale radius R_s . The density of X, \bar{X} and C particles inside the scale radius is

$$n_X + n_{\bar{X}} = f \frac{1}{m_X} \frac{M_s}{\frac{4}{3} \pi R_s^3} \quad (4.15)$$

$$n_C = f_{(XC)} (n_X + n_{\bar{X}}) \quad (4.16)$$

where we have expressed the density of C particles in terms of the asymmetry $f_{(XC)}$ defined in equation 3.2.

We assume Bremsstrahlung and Compton scattering off the dark CMB photons that can lead to cooling [1] (for a detailed analysis of cooling in the dark sector see [98]). The time scale for bremsstrahlung is,

$$t_{brem} = \frac{3}{16} \frac{n_X + n_{\bar{X}} + n_C}{(n_X + n_{\bar{X}}) n_C} \frac{m_C^{3/2} T_{vir}^{1/2}}{\alpha_D^3} \quad (4.17)$$

The Compton cooling off dark CMB occurs on a timescale

$$t_{comp} = \frac{135}{64\pi^3} \frac{n_X + n_{\bar{X}} + n_C}{n_C} \frac{m_C^3}{\alpha_D^2 (T_D^0 (1+z))^4} \quad (4.18)$$

The time scale for equilibration between X and C is

$$t_{eq} = \frac{m_X m_C}{2\sqrt{3}\pi\alpha_D^2} \frac{(E_C/m_C)^{3/2}}{n_C \log\left(1 + \frac{v_C^4 m_C^2}{\alpha_D^2 n_C^{2/3}}\right)} \quad (4.19)$$

If the C particles are in kinetic equilibrium with X and \bar{X} , i.e. the equilibration timescale is shorter than the cooling time scale, the cooled compact objects will be composed of all of X, \bar{X}, C particles. On the other hand, if $t_{eq} > t_{cool}$, then the C particles cool but cannot cool X and \bar{X} particles through equilibrium processes.

4.3 Direct detection

In principle, the kinetic mixing of the Z' with the photon in the portal models can give rise direct detection, which in principle could be a significant constraint. The direct detection constraints for millicharged dark matter (i.e. through the massless Z' portal) are very strong, with the WIMP-nucleon cross section estimated by

$$\sigma^{(n)} = \frac{Z^2}{A^2} \frac{16\pi\alpha^2\epsilon^2\mu_n^2}{q^4} \sim 10^{-45} \text{ cm}^2 \left(\frac{\epsilon}{10^{-10}}\right)^2 \left(\frac{30 \text{ MeV}}{q}\right)^4. \quad (4.20)$$

where q is the typical momentum transfer and Z and A are the atomic and mass number of the target. However, in much of the parameter space, the millicharged dark matter is evacuated from the disk by shock waves generated during supernova explosions, and is shielded from (re)entering the disk by the large-scale magnetic field of the galaxy [45, 99]. This mechanism is efficient for

$$5.4 \times 10^{-13} \frac{m_X}{\text{GeV}} < \epsilon < 3.4 \times 10^{-4} \sqrt{\frac{m_X}{\text{GeV}}} \quad (4.21)$$

which is a very large range of ϵ for $m_X \sim 30 \text{ GeV}$.

The constraints for the massive Z' portal depend on the mass of the Z' . For our case, where $m_{Z'} \gg q$, the direct detection cross section is,

$$\sigma^{(n)} = \frac{Z^2}{A^2} \frac{16\pi\alpha^2\epsilon^2\mu_n^2}{m_{Z'}^4} \sim 10^{-45} \text{ cm}^2 \left(\frac{\epsilon}{10^{-5}}\right)^2 \left(\frac{10 \text{ GeV}}{m_{Z'}}\right)^4. \quad (4.22)$$

In fact this constraint is further relaxed in our setup. The X, \bar{X} component of dark matter makes up only a fraction of the total dark matter. Most of X and \bar{X} are in collapsed objects, so the direct detection signal exists only if these objects overlap with our solar system. Finally, the velocity dispersion in the collapsed object is much lower than the velocity dispersion for the CDM halo, leading to typical recoil energies lower than the experimental threshold for most direct detection experiments. We conclude that direct detection does not put strong model-independent constraints on the model we are investigating.

4.4 Constraints on compact objects

We now estimate the size of compact objects in our models and evaluate existing constraints. We show these constraints in figure 8.

- **Total number**

Given a certain mass of the objects and the fraction of dark matter in the XC component, we can derive a bound on the number of such objects in our halo,

$$\mathcal{N}_{total} \lesssim 10^6 \left(\frac{f}{0.01} \right) \left(\frac{10^4 M_\odot}{M} \right) \left(\frac{M_{DM,total}}{10^{12} M_\odot} \right). \quad (4.23)$$

in the entire galaxy. If this bound is not saturated the rest of dissipative dark matter might be in more diffuse clouds.

- **Longevity**

The symmetric component in dense objects can annihilate, putting a constraint on the size of a dark photon gauge coupling for a given value of M and R . This constraint is relevant for the existence of compact objects even if there is no γ -ray signal.

$$n_X \sigma_{X\bar{X}} v = \frac{1 + f_{(XC)}}{2} \frac{M}{m_X \left(\frac{4}{3} \pi R^3 \right)} \left(\frac{\pi \alpha_D^2}{m_X^2} + \frac{\pi (\alpha_D + \alpha_{Z'})^2}{m_X^2} \right) S_{ann}(\alpha_D/c_{XC}) < H_0 \quad (4.24)$$

where we have ignored corrections of $\mathcal{O}(m_{Z'}/m_X)$, and S_{ann} is the Sommerfeld enhancement,

$$S_{ann}(\zeta) = \frac{2\pi\zeta}{1 - e^{-2\pi\zeta}}. \quad (4.25)$$

- **Further cooling**

If the virial velocity for a compact object is higher than the binding energy for the XC system, then there may be a non-negligible ionized C component, which can lead to further cooling and collapse. For a virially supported object, we can impose the following conservative bound,

$$T_{vir} = \frac{G_N M \mu}{5R} < \frac{1}{2} m_C \alpha_D^2. \quad (4.26)$$

We impose this constraint for our analysis, but in principle such objects can also be stabilized by other mechanisms. We are also ignoring other cooling processes such as atomic and molecular cooling which could cool the compact object further.

- **Tidal Stripping**

The tidal radius for a compact object of mass M at a distance r from the galactic center is,

$$R_{tidal} \simeq r \left(\frac{M}{3M_{enc}(r)} \right)^{\frac{1}{3}}. \quad (4.27)$$

Objects larger than this radius will be tidally disrupted. If the density profile of the compact object is constant, then objects of all size with the given density would not remain. But if the density towards the inner parts the compact object is higher, then tidal disruption can leave behind a dense core of the original object.

In the inner galaxy, the mass enclosed is dominated by baryons in the form of the bulge and the stellar disk. We use the parametrization of the bulge and disk from [100, 101],

$$\rho_B(b) = \frac{\rho_{B,0}}{\eta\zeta b_m^3} \frac{e^{-(b/b_m)^2}}{(1+b/b_0)^{1.8}} \quad (4.28)$$

with $b^2 = x^2 + (y/\eta)^2 + (z/\zeta)^2$, $\rho_{B,0} = 3.5 \times 10^{12} M_\odot$, $b_m = 1.9$ kpc, $b_0 = 0.1$ kpc, $\eta = 0.5$ and $\zeta = 0.6$.

The stellar disk is modeled as

$$\Sigma_\star(r) = \Sigma_0 e^{-r/r_d} \quad (4.29)$$

with $\Sigma_0 = 562 M_\odot/\text{pc}^2$ and scale radius $r_d = 3$ kpc. As a benchmark, we impose the constraint that the compact object is smaller than the tidal radius at ~ 0.3 kpc from the galactic center,

$$R \lesssim (0.3 \text{ kpc}) \left(\frac{M}{3M_{enc}(0.3 \text{ kpc})} \right)^{\frac{1}{3}}, \quad (4.30)$$

$$M_{enc}(0.3 \text{ kpc}) \simeq \int_0^{0.3 \text{ kpc}} dx dy dz \rho_B(b) + \int_0^{0.3 \text{ kpc}} 2\pi r' \Sigma_\star(r') dr' = 3 \times 10^8 M_\odot. \quad (4.31)$$

5 The Galactic Center Excess

A number of analyses have found that the FERMI telescope has observed an excess of gamma ray emission from the center of the galaxy [13–17]. There are also hints for excess gamma-ray emission from Andromeda [102] and from the dwarf galaxy Reticulum II [103–105]. The origin of the GC excess is intensely debated, but one exciting possibility is that it originates from dark matter annihilations [13–15, 64–66, 106–118].

However, Refs. [18, 19] showed that there are some hints for a statistical preference for point-source emission in the GCE (but this conclusion might be sensitive to structure in the diffuse background that is not modeled by the range of background models considered, see also [21]). The morphology of the excess if pointlike would be in tension with the smooth distribution expected for a CDM annihilation [20, 119]. Most physicists would then attribute the observed point-like spectrum to a new population of Millisecond Pulsars (MSPs) [20, 22]. We investigate the alternative possibility that these point sources could arise from dark matter annihilation in compact objects.

We highlight the parameters of our model that can reproduce this point source signal, specifically the mass m_X and the coupling $\alpha_{Z'}$, and the size of objects, $\{M, R\}$. We choose the simplified limit where all objects have similar masses and sizes, and have a uniform density. It would be straightforward to vary these assumptions to include any other mass function and a realistic density profile and distribution that might be motivated by N-body simulations. If there is a very sizeable spread in the mass function, there will be a large number of brighter compact objects, which should have been resolved as point sources by Fermi. We assume the spatial distribution of the compact objects in the inner galaxy to be spherically symmetric with an NFW-squared radial profile (more precisely $r^{-2.5}$) in the inner galaxy. This is motivated by the observed morphology of the galactic center excess.

The mass m_X can be fixed by finding the best-fit spectrum to the excess. The point source analysis in [18] uses a single wide energy bin, which is unsuitable for a spectral analysis. Instead we find the best-fit spectrum following the analysis in [16, 114]. We then consider the annihilation rate and the size and mass of compact objects required to reproduce the observed point-source excess.

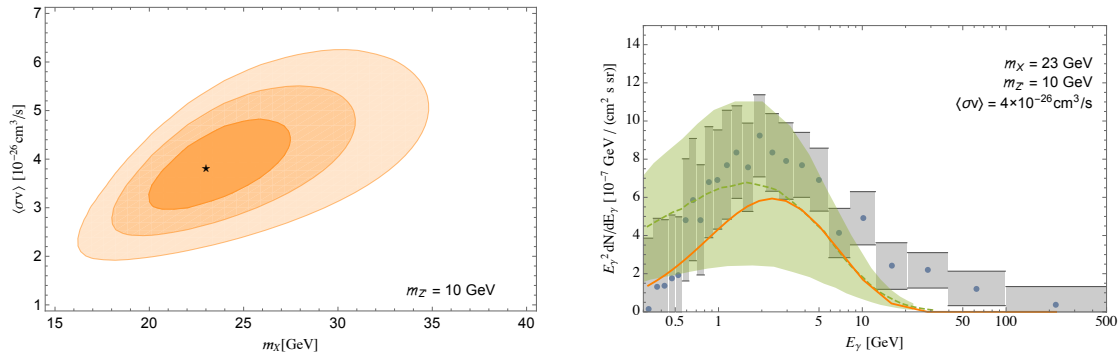


Figure 7: Left: We show 1, 2, 3 σ contours around the best-fit spectrum for the Z' model. Right: The spectrum of photons obtained for the best-fit point in our model (orange) overlaid with the spectrum for the excess from Calore et al [16] (gray) and recent Fermi results [20] (green). Note that the gray error bands are highly correlated, and the orange curve does fit the data reasonably well. For this plot we assume an NFW profile with a region of interest in [16, 114] with $J = 2.0 \times 10^{23} \text{ GeV}^2/\text{cm}^5$.

5.1 Spectrum for the Galactic Center excess

For the spectral fit in this section, we will follow the analysis of [16]. The region of interest (ROI) in this analysis extended to a $\pm 20^\circ$ square around the galactic center, with the inner 2° latitude masked out. We further choose an NFW profile ($\rho_\odot = 0.4 \text{ GeV}/\text{cm}^3$, $R_s = 20 \text{ kpc}$, $\gamma = 1.20$), which translates to $J = 2.0 \times 10^{23} \text{ GeV}^2/\text{cm}^5$.

The flux from DM annihilation with DM mass m_X is (for Dirac fermions)

$$\frac{d\Phi}{dE} = \frac{J\langle\sigma v\rangle}{16\pi m_X^2} \left\langle \frac{dN}{dE} \right\rangle \quad (5.1)$$

where the flux factor J is the line-of-sight integral of the dark matter density, and dN/dE is the spectrum of photons per annihilation. Given the J -factor and the spectrum per annihilation for different masses, we can in principle find the best-fit m_X and $\langle\sigma v\rangle$. We will use only the m_X value found this way, and our best-fit $\langle\sigma v\rangle$ will instead be determined by fitting to the point source flux in the next section.

When $\alpha_D > \alpha_{Z'}$, the dominant annihilation mode that produces photons is $X\bar{X} \rightarrow \gamma_D Z'$. The Z' then decays to SM fermions through the ϵ mixing which produces a continuum photon spectrum. The spectrum can be calculated by boosting the photons in the rest frame of the Z' to the galactic frame. The spectrum of photons produced in such cascade decays was also considered in a model-independent analysis in [120].

The spectrum of photons in the rest frame of Z' is

$$\left. \frac{dN(E)}{dE} \right|_{Z'} = \sum_f br(Z' \rightarrow f) \left. \frac{dN_f(E)}{dE} \right|_{Z'} \quad (5.2)$$

where the sum is over the spectrum from each of the decay modes of the Z' through the kinetic mixing [83], and $\left. \frac{dN_f(E)}{dE} \right|_{Z'}$ is the spectrum of photons from decay $Z' \rightarrow f$. The spectrum from various standard model final states can be simulated using PYTHIA [121, 122], and has been tabulated in PPPC 4 DM ID [123, 124].

The spectrum of photons per annihilation, in the galactic frame, is obtained by convolving the spectrum in the rest frame of Z' with a unit normalized “box” [114]

$$\left\langle \frac{dN(E)}{dE} \right\rangle = \frac{1}{x_+ - x_-} \int_{E_{x_-}}^{E_{x_+}} \frac{dE'}{E'} \frac{dN(E')}{dE'} \Big|_{Z'} , \quad (5.3)$$

and

$$x_{\pm} = \frac{4m_X^2 + m_{Z'}^2}{4m_X m_{Z'}} \left(1 \pm \frac{4m_X^2 - m_{Z'}^2}{4m_X^2 + m_{Z'}^2} \right) \quad (5.4)$$

In figure 7 we show the χ^2 -contours for the photon spectrum fit to the observed excess, as a function of the dark matter mass and the cross section (given the astrophysical J -factor) and the spectrum of the best-fit point. The best fit dark matter mass for our model, $m_X \simeq 25$ GeV is seen to provide a good fit to the observed spectrum of the excess.

5.2 The Point-like GeV Excess from Compact Objects in Dissipative Dark Matter

According to [18] (see also [19, 20]), the signal appears to originate from point-like sources that are distributed with an NFW-squared profile. The region of interest for this analysis was taken to be inner 30° with $|b| < 2^\circ$ masked. The pixel size for the analyses is 0.5° to a side, which translates to about 75 pc at the center of the galaxy. The point spread function varies between 0.05° to 0.2° for the energy range 1–10 GeV. Therefore, any objects smaller than about 10 – 100 pc would give rise to non-Poissonian photon statistics, appearing as point sources. We saw in section 2.1 that for our chosen parameters we expect our compact objects to be $\mathcal{O}(10\text{--}100)$ pc in size, and hence to appear as point sources.

The analysis predicts a certain number of objects in the inner galaxy to account for the total flux absorbed by the point source template. In the inner 10° of the galaxy with $|b| \geq 2^\circ$, 86_{-25}^{+32} point sources can explain about half of the excess from the galactic center when the Fermi 3FGL point sources are masked. For the unmasked analysis in [18] the corresponding number is 132_{-25}^{+31} .

We note that the flux and the number of objects is roughly fixed independently in addition to being constrained by the total amount of flux. If we had a much larger number of objects (with a corresponding smaller flux per object), they would have photon-per-pixel statistics closer to a smooth morphology predicted by standard CDM substructure. Much fewer objects would need to be brighter to account for the total flux, and hence would be above the threshold for detection as point sources by Fermi.

We next turn to the normalization of our signal, which we fit to [18]. The normalization depends on the J -factor, on the total annihilation cross section $\langle\sigma v\rangle$ and on the number of photons per annihilation.

$$\Phi = \frac{\langle\sigma v\rangle J}{16\pi m_X^2} \langle N_\gamma \rangle \quad (5.5)$$

$$\langle N_\gamma \rangle \equiv \int_{E_{min}}^{E_{max}} dE \left\langle \frac{dN}{dE} \right\rangle \quad (5.6)$$

The total annihilation rate $X\bar{X} \rightarrow Z'\gamma_D$ is

$$\langle\sigma v\rangle = \frac{\pi\alpha_{Z'}\alpha_D}{m_X^2} S_{ann}(\alpha_D/c_{XC}) \quad (5.7)$$

to leading order in $m_{Z'}/m_X$. The velocity of dark matter in the compact object (c_{XC}) is given in equation 2.4.

In this analysis, a single energy bin from 1.893–11.943 GeV was used. For $m_X = 25$ GeV, $m_{Z'} = 10$ GeV, this corresponds to,

$$\langle N_\gamma \rangle \simeq 1.8 \quad (5.8)$$

The J -factor associated with the point sources is given by,

$$J = \sum_i^{\mathcal{N}} J_i = \mathcal{N}_{src} \bar{J} \quad (5.9)$$

where \bar{J} is the J -factor for each point source if they are all identical. In the analysis of [18], the flux from each source was estimated to be $\bar{\Phi} = 1.4 \pm 0.3 \times 10^{-10}$ photons/cm²/s. The J -factor for each point source is

$$\bar{J} = \left(1 - f_{(XC)}^2\right) \left(\frac{M^2}{\frac{4}{3}\pi R^3}\right) \frac{1}{r_\odot^2} \quad (5.10)$$

where $f_{(XC)}$ is the fraction of the dissipative component in bound states. The flux from each point source is,

$$\begin{aligned} \bar{\Phi} &= \frac{\langle \sigma v \rangle \bar{J}}{16\pi m_X^2} \langle N_\gamma \rangle \quad (5.11) \\ &\simeq 1 \times 10^{-10} \frac{1}{\text{cm}^2 \text{s}} \left(1 - f_{(XC)}^2\right) \left(\frac{10 \text{ pc}}{R}\right)^3 \left(\frac{M}{10^4 M_\odot}\right)^2 \left(\frac{25 \text{ GeV}}{m_X}\right)^2 \left(\frac{\langle \sigma v \rangle}{1.4 \times 10^{-24} \text{ cm}^3/\text{s}}\right) \left(\frac{\langle N_\gamma \rangle}{1.8}\right) \quad (5.12) \end{aligned}$$

where the numerical prefactor above is the consistent with the typical flux from a point source in the analysis of [18, 62]. The value of $\langle \sigma v \rangle$ is enhanced by the Sommerfeld effect, and therefore can be much larger today than the canonical thermal freezeout value of 2.2×10^{-26} cm³/s without affecting the relic abundance calculation.

In figure 8 we see the parameter space where the dark matter annihilations can explain the GCE. We also show constraints on the parameter space where the compact objects can undergo tidal disruption, annihilate away within the age of the universe, or are unstable to further cooling. We also show benchmark points from our instability analysis in section 2 for a few choices of the local dark disk density.

As noted above, we need an $\mathcal{O}(100)$ compact objects of mass $10^4 M_\odot$ each to account for the total flux of the GCE. For a CDM component with an NFW profile the total mass of dark matter in the inner galaxy region is $\sim 10^9 M_\odot$. Therefore, XC dark matter can be as little as 10^{-3} of the total dark matter in the inner galaxy while still giving us interesting signals. Intriguingly, the benchmark values from our stability analysis, $\Sigma_{XC,\odot} \sim 1\text{--}10 M_\odot/\text{pc}^2$, translate into a total dark disk mass of $10^9\text{--}10^{10} M_\odot$, or $10^{-3}\text{--}10^{-2}$ fraction of the total galactic dark matter.

6 Conclusion

Dissipative dark matter models can give rise to clumps of dark matter with enhanced density. Even if dissipative dark matter makes up a tiny fraction of the total dark matter density, these clumps can be the dominant site of annihilation, leading to novel indirect detection signatures.

We have considered a simple example of such a dissipative dark matter model and estimated the size and mass of collapsed objects we might expect as a function of the model parameters. We

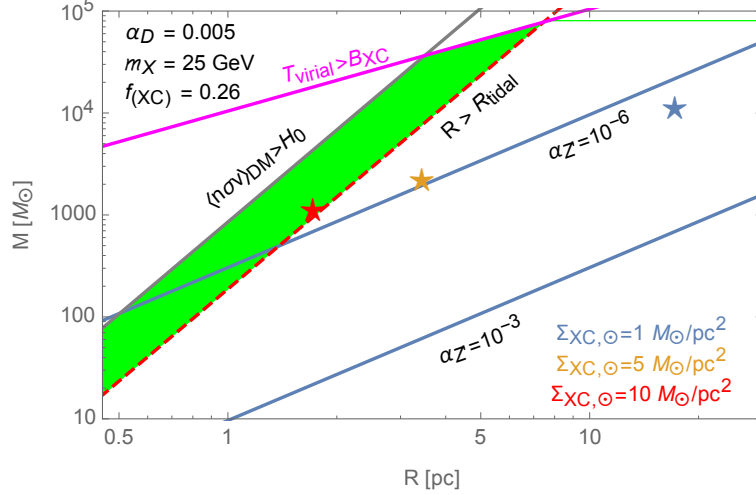


Figure 8: We show constraints on compact objects as a function of their mass M and radius R . The green shaded region is the preferred region for our analysis. In the region above the gray curve \bar{X} annihilates away within the lifetime of the universe. The region above the magenta line has $T_{\text{virial}} > B_{XC}$, so that the compact object would be unstable to further cooling. Objects to the right of the red dashed line can be tidally disrupted in the inner galaxy. The blue lines are contours of $\alpha_{Z'}$ to obtain the galactic center excess flux from $X\bar{X} \rightarrow Z'\gamma_D$ annihilation. We indicate a few benchmark values of $\{M, R\}$ (stars) which are estimates of the mass and size of compact objects we get from fragmentation for a given dark disk column density.

have shown that these objects could be small enough to appear as point sources in Fermi-LAT. The spectrum depends on the portal connecting the dark sector with the Standard Model.

With an additional massless dark photon, dark matter particles can annihilate to photon and a dark photon, which appear as a line spectrum in Fermi-LAT. A line from point sources would be a smoking gun signal of dissipative dark matter models. If the portal is a massive vector, the annihilation then leads to continuum photons, with a spectrum of that resembles the spectrum of photons from the $b\bar{b}$ final state. This can potentially provide an explanation of the point-source origin of the galactic center excess as arising from dark matter annihilation in these objects.

The point source morphology and continuum spectrum of gamma rays are characteristic signals of millisecond pulsars but as we have shown might possibly occur in certain classes of dark matter models. Our analysis gives us a target which we can try and distinguish from MSPs.

The authors of [125] consider observations of pulsars in other wavelengths and conclude that pulsar surveys in the radio frequencies will potentially be able to detect millisecond pulsars in the bulge. The absence of any signal in other wavelengths will strength to the hypothesis of dark matter compact objects as the origin of this signal.

The angular size of dark matter clouds in the inner galaxy can be comparable to the resolution of Fermi. If there are larger clouds, or clouds closer to us, Fermi-LAT might be able to resolve the structure, definitively discriminating it from pulsars.

UCMHs that form from large fluctuations in the power spectrum have also been considered as potential dark point sources [24–33]. For the UCMH, in addition to annihilation of dark matter within the UCMH, there will be annihilations of dark matter in the UCMH and in halo, leading to a

different radial dependence of the excess. There will also be annihilations in the halo with a diffuse morphology. These features will help distinguish UCMHs from dissipative compact objects. Further, due to dissipation the compact objects considered in this paper will be concentrated towards the center of the halo (possibly along a plane), whereas we expect UCMHs to be isotropically distributed throughout the halo.

Very little is known about dark matter, and even less about components which might be a small fraction. However, it is precisely these small but interesting components – not unlike baryons – which might provide the most spectacular signals from dark matter.

Acknowledgments

We thank Mariangela Lisanti for very useful comments on an earlier version of this manuscript. We are grateful to Francis-Yan Cyr-Racine, Matt Reece and Jakub Scholtz for discussions and comments on the manuscript. This work is supported by NSF grants PHY-0855591 and PHY-1216270.

References

- [1] J. Fan, A. Katz, L. Randall, and M. Reece, “Double-Disk Dark Matter,” *Phys. Dark Univ.* **2** (2013) 139–156, [arXiv:1303.1521 \[astro-ph.CO\]](#).
- [2] J. Fan, A. Katz, L. Randall, and M. Reece, “Dark-Disk Universe,” *Phys. Rev. Lett.* **110** no. 21, (2013) 211302, [arXiv:1303.3271 \[hep-ph\]](#).
- [3] F.-Y. Cyr-Racine and K. Sigurdson, “Cosmology of atomic dark matter,” *Phys. Rev.* **D87** no. 10, (2013) 103515, [arXiv:1209.5752 \[astro-ph.CO\]](#).
- [4] M. McCullough and L. Randall, “Exothermic Double-Disk Dark Matter,” *JCAP* **1310** (2013) 058, [arXiv:1307.4095 \[hep-ph\]](#).
- [5] J. Fan, A. Katz, and J. Shelton, “Direct and indirect detection of dissipative dark matter,” *JCAP* **1406** (2014) 059, [arXiv:1312.1336 \[hep-ph\]](#).
- [6] W. Fischler, D. Lorshbough, and W. Tangarife, “Supersymmetric Partially Interacting Dark Matter,” *Phys. Rev.* **D91** no. 2, (2015) 025010, [arXiv:1405.7708 \[hep-ph\]](#).
- [7] L. Randall and M. Reece, “Dark Matter as a Trigger for Periodic Comet Impacts,” *Physical Review Letters* **112** no. 16, (Apr., 2014) 161301, [arXiv:1403.0576](#).
- [8] L. Randall and J. Scholtz, “Dissipative Dark Matter and the Andromeda Plane of Satellites,” *JCAP* **1509** no. 09, (2015) 057, [arXiv:1412.1839 \[astro-ph.GA\]](#).
- [9] M. Reece and T. Roxlo, “Nonthermal production of dark radiation and dark matter,” *JHEP* **09** (2016) 096, [arXiv:1511.06768 \[hep-ph\]](#).
- [10] E. D. Kramer and L. Randall, “Interstellar Gas and a Dark Disk,” *Astrophys. J.* **829** no. 2, (2016) 126, [arXiv:1603.03058 \[astro-ph.GA\]](#).
- [11] E. D. Kramer and L. Randall, “Updated Kinematic Constraints on a Dark Disk,” *Astrophys. J.* **824** no. 2, (2016) 116, [arXiv:1604.01407 \[astro-ph.GA\]](#).
- [12] P. Agrawal, F.-Y. Cyr-Racine, L. Randall, and J. Scholtz, “Dark Catalysis,” [arXiv:1702.05482 \[astro-ph.CO\]](#).
- [13] L. Goodenough and D. Hooper, “Possible Evidence For Dark Matter Annihilation In The Inner Milky Way From The Fermi Gamma Ray Space Telescope,” [arXiv:0910.2998 \[hep-ph\]](#).

- [14] D. Hooper and L. Goodenough, “Dark Matter Annihilation in The Galactic Center As Seen by the Fermi Gamma Ray Space Telescope,” *Phys.Lett.* **B697** (2011) 412–428, [arXiv:1010.2752 \[hep-ph\]](#).
- [15] T. Daylan, D. P. Finkbeiner, D. Hooper, T. Linden, S. K. N. Portillo, N. L. Rodd, and T. R. Slatyer, “The characterization of the gamma-ray signal from the central Milky Way: A case for annihilating dark matter,” *Phys. Dark Univ.* **12** (2016) 1–23, [arXiv:1402.6703 \[astro-ph.HE\]](#).
- [16] F. Calore, I. Cholis, and C. Weniger, “Background model systematics for the Fermi GeV excess,” *JCAP* **1503** (2015) 038, [arXiv:1409.0042 \[astro-ph.CO\]](#).
- [17] **Fermi-LAT** Collaboration, M. Ajello *et al.*, “Fermi-LAT Observations of High-Energy γ -Ray Emission Toward the Galactic Center,” *Astrophys. J.* **819** no. 1, (2016) 44, [arXiv:1511.02938 \[astro-ph.HE\]](#).
- [18] S. K. Lee, M. Lisanti, B. R. Safdi, T. R. Slatyer, and W. Xue, “Evidence for Unresolved γ -Ray Point Sources in the Inner Galaxy,” *Phys. Rev. Lett.* **116** no. 5, (2016) 051103, [arXiv:1506.05124 \[astro-ph.HE\]](#).
- [19] R. Bartels, S. Krishnamurthy, and C. Weniger, “Strong support for the millisecond pulsar origin of the Galactic center GeV excess,” *Phys. Rev. Lett.* **116** no. 5, (2016) 051102, [arXiv:1506.05104 \[astro-ph.HE\]](#).
- [20] **Fermi-LAT** Collaboration, M. Ajello *et al.*, “Characterizing the population of pulsars in the Galactic bulge with the *Fermi* Large Area Telescope,” *Submitted to: Astrophys. J.* (2017) , [arXiv:1705.00009 \[astro-ph.HE\]](#).
- [21] S. Horiuchi, M. Kaplinghat, and A. Kwa, “Investigating the Uniformity of the Excess Gamma rays towards the Galactic Center Region,” [arXiv:1604.01402 \[astro-ph.HE\]](#).
- [22] T. D. Brandt and B. Kocsis, “Disrupted Globular Clusters Can Explain the Galactic Center Gamma Ray Excess,” *Astrophys. J.* **812** no. 1, (2015) 15, [arXiv:1507.05616 \[astro-ph.HE\]](#).
- [23] D. Hooper and T. Linden, “The Gamma-Ray Pulsar Population of Globular Clusters: Implications for the GeV Excess,” *JCAP* **1608** no. 08, (2016) 018, [arXiv:1606.09250 \[astro-ph.HE\]](#).
- [24] V. Berezhinsky, V. Dokuchaev, and Y. Eroshenko, “Small - scale clumps in the galactic halo and dark matter annihilation,” *Phys. Rev.* **D68** (2003) 103003, [arXiv:astro-ph/0301551 \[astro-ph\]](#).
- [25] M. Ricotti and A. Gould, “A New Probe of Dark Matter and High-Energy Universe Using Microlensing,” *Astrophys. J.* **707** (2009) 979–987, [arXiv:0908.0735 \[astro-ph.CO\]](#).
- [26] P. Scott and S. Sivertsson, “Gamma-Rays from Ultracompact Primordial Dark Matter Minihalos,” *Phys. Rev. Lett.* **103** (2009) 211301, [arXiv:0908.4082 \[astro-ph.CO\]](#). [Erratum: *Phys. Rev. Lett.*105,119902(2010)].
- [27] A. S. Josan and A. M. Green, “Gamma-rays from ultracompact minihalos: potential constraints on the primordial curvature perturbation,” *Phys. Rev.* **D82** (2010) 083527, [arXiv:1006.4970 \[astro-ph.CO\]](#).
- [28] A. L. Erickcek and K. Sigurdson, “Reheating Effects in the Matter Power Spectrum and Implications for Substructure,” *Phys. Rev.* **D84** (2011) 083503, [arXiv:1106.0536 \[astro-ph.CO\]](#).
- [29] T. Bringmann, P. Scott, and Y. Akrami, “Improved constraints on the primordial power spectrum at small scales from ultracompact minihalos,” *Phys. Rev.* **D85** (2012) 125027, [arXiv:1110.2484 \[astro-ph.CO\]](#).
- [30] V. S. Berezhinsky, V. I. Dokuchaev, and Yu. N. Eroshenko, “Formation and internal structure of superdense dark matter clumps and ultracompact minihaloes,” *JCAP* **1311** (2013) 059, [arXiv:1308.6742 \[astro-ph.CO\]](#).
- [31] H. A. Clark, G. F. Lewis, and P. Scott, “Investigating dark matter substructure with pulsar timing I.

- Constraints on ultracompact minihaloes,” *Mon. Not. Roy. Astron. Soc.* **456** no. 2, (2016) 1394–1401, [arXiv:1509.02938 \[astro-ph.CO\]](#). [Erratum: *Mon. Not. Roy. Astron. Soc.* 464,no.2,2468(2017)].
- [32] G. Aslanyan, L. C. Price, J. Adams, T. Bringmann, H. A. Clark, R. Easther, G. F. Lewis, and P. Scott, “Ultracompact minihalos as probes of inflationary cosmology,” *Phys. Rev. Lett.* **117** no. 14, (2016) 141102, [arXiv:1512.04597 \[astro-ph.CO\]](#).
- [33] H. A. Clark, N. Iwanus, P. J. Elahi, G. F. Lewis, and P. Scott, “Heating of galactic gas by dark matter annihilation in ultracompact minihalos,” *JCAP* **1705** no. 05, (2017) 048, [arXiv:1611.08619 \[astro-ph.CO\]](#).
- [34] A. B. Romeo, “Stability of thick two-component galactic discs,” *MNRAS* **256** (May, 1992) 307–320.
- [35] R. R. Rafikov, “The local axisymmetric instability criterion in a thin, rotating, multicomponent disc,” *MNRAS* **323** (May, 2001) 445–452, [astro-ph/0007058](#).
- [36] J. Binney and S. Tremaine, *Galactic dynamics*. Princeton University Press, Princeton, 2008.
- [37] N. J. Shaviv, “The Paleoclimatic evidence for Strongly Interacting Dark Matter Present in the Galactic Disk,” [arXiv:1606.02851 \[astro-ph.GA\]](#).
- [38] C. F. McKee, A. Parravano, and D. J. Hollenbach, “Stars, Gas, and Dark Matter in the Solar Neighborhood,” *ApJ* **814** (Nov., 2015) 13, [arXiv:1509.05334](#).
- [39] J. M. Cline, Z. Liu, and W. Xue, “Millicharged Atomic Dark Matter,” *Phys. Rev.* **D85** (2012) 101302, [arXiv:1201.4858 \[hep-ph\]](#).
- [40] L. B. Okun, “LIMITS OF ELECTRODYNAMICS: PARAPHOTONS?,” *Sov. Phys. JETP* **56** (1982) 502. [*Zh. Eksp. Teor. Fiz.* 83,892(1982)].
- [41] B. Holdom, “Two $U(1)$ ’s and Epsilon Charge Shifts,” *Phys. Lett.* **B166** (1986) 196–198.
- [42] S. Davidson, B. Campbell, and D. C. Bailey, “Limits on particles of small electric charge,” *Phys. Rev.* **D43** (1991) 2314–2321.
- [43] S. Davidson, S. Hannestad, and G. Raffelt, “Updated bounds on millicharged particles,” *JHEP* **05** (2000) 003, [arXiv:hep-ph/0001179 \[hep-ph\]](#).
- [44] S. L. Dubovsky, D. S. Gorbunov, and G. I. Rubtsov, “Narrowing the window for millicharged particles by CMB anisotropy,” *JETP Lett.* **79** (2004) 1–5, [arXiv:hep-ph/0311189 \[hep-ph\]](#). [*Pisma Zh. Eksp. Teor. Fiz.* 79,3(2004)].
- [45] S. D. McDermott, H.-B. Yu, and K. M. Zurek, “Turning off the Lights: How Dark is Dark Matter?,” *Phys. Rev.* **D83** (2011) 063509, [arXiv:1011.2907 \[hep-ph\]](#).
- [46] R. J. Wilkinson, J. Lesgourgues, and C. Boehm, “Using the CMB angular power spectrum to study Dark Matter-photon interactions,” *JCAP* **1404** (2014) 026, [arXiv:1309.7588 \[astro-ph.CO\]](#).
- [47] A. D. Dolgov, S. L. Dubovsky, G. I. Rubtsov, and I. I. Tkachev, “Constraints on millicharged particles from Planck data,” *Phys. Rev.* **D88** no. 11, (2013) 117701, [arXiv:1310.2376 \[hep-ph\]](#).
- [48] C. Brust, D. E. Kaplan, and M. T. Walters, “New Light Species and the CMB,” *JHEP* **12** (2013) 058, [arXiv:1303.5379 \[hep-ph\]](#).
- [49] C. Dvorkin, K. Blum, and M. Kamionkowski, “Constraining Dark Matter-Baryon Scattering with Linear Cosmology,” *Phys. Rev.* **D89** no. 2, (2014) 023519, [arXiv:1311.2937 \[astro-ph.CO\]](#).
- [50] H. Vogel and J. Redondo, “Dark Radiation constraints on minicharged particles in models with a hidden photon,” *JCAP* **1402** (2014) 029, [arXiv:1311.2600 \[hep-ph\]](#).
- [51] N. Vinyoles and H. Vogel, “Minicharged Particles from the Sun: A Cutting-Edge Bound,” *JCAP* **1603** no. 03, (2016) 002, [arXiv:1511.01122 \[hep-ph\]](#).

- [52] J. B. Muoz, E. D. Kovetz, and Y. Ali-Hamoud, “Heating of Baryons due to Scattering with Dark Matter During the Dark Ages,” *Phys. Rev.* **D92** no. 8, (2015) 083528, [arXiv:1509.00029 \[astro-ph.CO\]](#).
- [53] Y. Ali-Hamoud, J. Chluba, and M. Kamionkowski, “Constraints on Dark Matter Interactions with Standard Model Particles from Cosmic Microwave Background Spectral Distortions,” *Phys. Rev. Lett.* **115** no. 7, (2015) 071304, [arXiv:1506.04745 \[astro-ph.CO\]](#).
- [54] K. Kadota, T. Sekiguchi, and H. Tashiro, “A new constraint on millicharged dark matter from galaxy clusters,” [arXiv:1602.04009 \[astro-ph.CO\]](#).
- [55] A. Kamada, K. Kohri, T. Takahashi, and N. Yoshida, “Effects of electrically charged dark matter on cosmic microwave background anisotropies,” *Phys. Rev.* **D95** no. 2, (2017) 023502, [arXiv:1604.07926 \[astro-ph.CO\]](#).
- [56] A. A. Prinz *et al.*, “Search for millicharged particles at SLAC,” *Phys. Rev. Lett.* **81** (1998) 1175–1178, [arXiv:hep-ex/9804008 \[hep-ex\]](#).
- [57] J. Jaeckel, M. Jankowiak, and M. Spannowsky, “LHC probes the hidden sector,” *Phys. Dark Univ.* **2** (2013) 111–117, [arXiv:1212.3620 \[hep-ph\]](#).
- [58] A. Haas, C. S. Hill, E. Izaguirre, and I. Yavin, “Looking for milli-charged particles with a new experiment at the LHC,” *Phys. Lett.* **B746** (2015) 117–120, [arXiv:1410.6816 \[hep-ph\]](#).
- [59] E. Gabrielli, L. Marzola, E. Milotti, and H. Veerme, “Polarization observables for millicharged particles in photon collisions,” *Phys. Rev.* **D94** no. 9, (2016) 095014, [arXiv:1604.00393 \[hep-ph\]](#).
- [60] C. El Aisati, T. Hambye, and T. Scarn, “Can a millicharged dark matter particle emit an observable gamma-ray line?,” *JHEP* **08** (2014) 133, [arXiv:1403.1280 \[hep-ph\]](#).
- [61] **Fermi-LAT** Collaboration, M. Ackermann *et al.*, “Updated search for spectral lines from Galactic dark matter interactions with pass 8 data from the Fermi Large Area Telescope,” *Phys. Rev.* **D91** no. 12, (2015) 122002, [arXiv:1506.00013 \[astro-ph.HE\]](#).
- [62] S. K. Lee, M. Lisanti, and B. R. Safdi, “Distinguishing Dark Matter from Unresolved Point Sources in the Inner Galaxy with Photon Statistics,” *JCAP* **1505** no. 05, (2015) 056, [arXiv:1412.6099 \[astro-ph.CO\]](#).
- [63] E. Izaguirre and I. Yavin, “New window to millicharged particles at the LHC,” *Phys. Rev.* **D92** no. 3, (2015) 035014, [arXiv:1506.04760 \[hep-ph\]](#).
- [64] A. Berlin, D. Hooper, and S. D. McDermott, “Simplified Dark Matter Models for the Galactic Center Gamma-Ray Excess,” *Phys. Rev.* **D89** no. 11, (2014) 115022, [arXiv:1404.0022 \[hep-ph\]](#).
- [65] P. Agrawal, B. Batell, D. Hooper, and T. Lin, “Flavored Dark Matter and the Galactic Center Gamma-Ray Excess,” *Phys. Rev.* **D90** no. 6, (2014) 063512, [arXiv:1404.1373 \[hep-ph\]](#).
- [66] E. Izaguirre, G. Krnjaic, and B. Shuve, “The Galactic Center Excess from the Bottom Up,” *Phys. Rev.* **D90** no. 5, (2014) 055002, [arXiv:1404.2018 \[hep-ph\]](#).
- [67] E. M. Riordan *et al.*, “A Search for Short Lived Axions in an Electron Beam Dump Experiment,” *Phys. Rev. Lett.* **59** (1987) 755.
- [68] J. D. Bjorken, S. Ecklund, W. R. Nelson, A. Abashian, C. Church, B. Lu, L. W. Mo, T. A. Nunamaker, and P. Rassmann, “Search for Neutral Metastable Penetrating Particles Produced in the SLAC Beam Dump,” *Phys. Rev.* **D38** (1988) 3375.
- [69] A. Bross, M. Crisler, S. H. Pordes, J. Volk, S. Errede, and J. Wrbanek, “A Search for Shortlived Particles Produced in an Electron Beam Dump,” *Phys. Rev. Lett.* **67** (1991) 2942–2945.

- [70] J. Blumlein and J. Brunner, “New Exclusion Limits for Dark Gauge Forces from Beam-Dump Data,” *Phys. Lett.* **B701** (2011) 155–159, [arXiv:1104.2747 \[hep-ex\]](#).
- [71] S. Andreas, C. Niebuhr, and A. Ringwald, “New Limits on Hidden Photons from Past Electron Beam Dumps,” *Phys. Rev.* **D86** (2012) 095019, [arXiv:1209.6083 \[hep-ph\]](#).
- [72] J. B. Dent, F. Ferrer, and L. M. Krauss, “Constraints on Light Hidden Sector Gauge Bosons from Supernova Cooling,” [arXiv:1201.2683 \[astro-ph.CO\]](#).
- [73] D. Kazanas, R. N. Mohapatra, S. Nussinov, V. L. Teplitz, and Y. Zhang, “Supernova Bounds on the Dark Photon Using its Electromagnetic Decay,” *Nucl. Phys.* **B890** (2014) 17–29, [arXiv:1410.0221 \[hep-ph\]](#).
- [74] **BaBar** Collaboration, J. P. Lees *et al.*, “Search for a Dark Photon in e^+e^- Collisions at BaBar,” *Phys. Rev. Lett.* **113** no. 20, (2014) 201801, [arXiv:1406.2980 \[hep-ex\]](#).
- [75] **A1** Collaboration, H. Merkel *et al.*, “Search for Light Gauge Bosons of the Dark Sector at the Mainz Microtron,” *Phys. Rev. Lett.* **106** (2011) 251802, [arXiv:1101.4091 \[nucl-ex\]](#).
- [76] **KLOE-2** Collaboration, F. Archilli *et al.*, “Search for a vector gauge boson in ϕ meson decays with the KLOE detector,” *Phys. Lett.* **B706** (2012) 251–255, [arXiv:1110.0411 \[hep-ex\]](#).
- [77] **KLOE-2** Collaboration, D. Babusci *et al.*, “Limit on the production of a light vector gauge boson in phi meson decays with the KLOE detector,” *Phys. Lett.* **B720** (2013) 111–115, [arXiv:1210.3927 \[hep-ex\]](#).
- [78] **KLOE-2** Collaboration, D. Babusci *et al.*, “Search for light vector boson production in $e^+e^- \rightarrow \mu^+\mu^-\gamma$ interactions with the KLOE experiment,” *Phys. Lett.* **B736** (2014) 459–464, [arXiv:1404.7772 \[hep-ex\]](#).
- [79] **KLOE-2** Collaboration, A. Anastasi *et al.*, “Limit on the production of a new vector boson in $e^+e^- \rightarrow U\gamma$, $U \rightarrow \pi^+\pi^-$ with the KLOE experiment,” *Phys. Lett.* **B757** (2016) 356–361, [arXiv:1603.06086 \[hep-ex\]](#).
- [80] M. Endo, K. Hamaguchi, and G. Mishima, “Constraints on Hidden Photon Models from Electron g-2 and Hydrogen Spectroscopy,” *Phys. Rev.* **D86** (2012) 095029, [arXiv:1209.2558 \[hep-ph\]](#).
- [81] **ACME** Collaboration, J. Baron *et al.*, “Order of Magnitude Smaller Limit on the Electric Dipole Moment of the Electron,” *Science* **343** (2014) 269–272, [arXiv:1310.7534 \[physics.atom-ph\]](#).
- [82] **NA48/2** Collaboration, J. R. Batley *et al.*, “Search for the dark photon in π^0 decays,” *Phys. Lett.* **B746** (2015) 178–185, [arXiv:1504.00607 \[hep-ex\]](#).
- [83] D. Curtin, R. Essig, S. Gori, and J. Shelton, “Illuminating Dark Photons with High-Energy Colliders,” *JHEP* **02** (2015) 157, [arXiv:1412.0018 \[hep-ph\]](#).
- [84] I. Hoenig, G. Samach, and D. Tucker-Smith, “Searching for dilepton resonances below the Z mass at the LHC,” *Phys. Rev.* **D90** no. 7, (2014) 075016, [arXiv:1408.1075 \[hep-ph\]](#).
- [85] J. Alexander *et al.*, “Dark Sectors 2016 Workshop: Community Report,” 2016. [arXiv:1608.08632 \[hep-ph\]](#).
- [86] B. Echenard, R. Essig, and Y.-M. Zhong, “Projections for Dark Photon Searches at Mu3e,” *JHEP* **01** (2015) 113, [arXiv:1411.1770 \[hep-ph\]](#).
- [87] M. Battaglieri *et al.*, “The Heavy Photon Search Test Detector,” *Nucl. Instrum. Meth.* **A777** (2015) 91–101, [arXiv:1406.6115 \[physics.ins-det\]](#).
- [88] J. Balewski *et al.*, “DarkLight: A Search for Dark Forces at the Jefferson Laboratory Free-Electron Laser Facility,” in *Proceedings, 2013 Community Summer Study on the Future of U.S. Particle*

Physics: Snowmass on the Mississippi (CSS2013): Minneapolis, MN, USA, July 29-August 6, 2013. 2013. [arXiv:1307.4432 \[physics.ins-det\]](#).

https://misportal.jlab.org/ul/publications/view_pub.cfm?pub_id=12467.

- [89] **APEX** Collaboration, S. Abrahamyan *et al.*, “Search for a New Gauge Boson in Electron-Nucleus Fixed-Target Scattering by the APEX Experiment,” *Phys. Rev. Lett.* **107** (2011) 191804, [arXiv:1108.2750 \[hep-ex\]](#).
- [90] R. Essig, P. Schuster, N. Toro, and B. Wojtsekhowski, “An Electron Fixed Target Experiment to Search for a New Vector Boson A' Decaying to $e+e^-$,” *JHEP* **02** (2011) 009, [arXiv:1001.2557 \[hep-ph\]](#).
- [91] J. D. Bjorken, R. Essig, P. Schuster, and N. Toro, “New Fixed-Target Experiments to Search for Dark Gauge Forces,” *Phys. Rev.* **D80** (2009) 075018, [arXiv:0906.0580 \[hep-ph\]](#).
- [92] **SHiP** Collaboration, M. Anelli *et al.*, “A facility to Search for Hidden Particles (SHiP) at the CERN SPS,” [arXiv:1504.04956 \[physics.ins-det\]](#).
- [93] P. Agrawal, F.-Y. Cyr-Racine, L. Randall, and J. Scholtz, “Make Dark Matter Charged Again,” [arXiv:1610.04611 \[hep-ph\]](#).
- [94] J. L. Feng, H. Tu, and H.-B. Yu, “Thermal Relics in Hidden Sectors,” *JCAP* **0810** (2008) 043, [arXiv:0808.2318 \[hep-ph\]](#).
- [95] M. L. Graesser, I. M. Shoemaker, and L. Vecchi, “Asymmetric WIMP dark matter,” *JHEP* **10** (2011) 110, [arXiv:1103.2771 \[hep-ph\]](#).
- [96] I. Baldes and K. Petraki, “Asymmetric thermal-relic dark matter: Sommerfeld-enhanced freeze-out, annihilation signals and unitarity bounds,” [arXiv:1703.00478 \[hep-ph\]](#).
- [97] P. Gondolo, J. Edsjo, P. Ullio, L. Bergstrom, M. Schelke, and E. A. Baltz, “DarkSUSY: Computing supersymmetric dark matter properties numerically,” *JCAP* **0407** (2004) 008, [arXiv:astro-ph/0406204 \[astro-ph\]](#).
- [98] E. Rosenberg and J. Fan, “Cooling in a Dissipative Dark Sector,” [arXiv:1705.10341 \[astro-ph.GA\]](#).
- [99] L. Chuzhoy and E. W. Kolb, “Reopening the window on charged dark matter,” *JCAP* **0907** (2009) 014, [arXiv:0809.0436 \[astro-ph\]](#).
- [100] J. Binney, O. Gerhard, and D. Spergel, “The photometric structure of the inner galaxy,” *Mon. Not. Roy. Astron. Soc.* **288** (1997) 365–374, [arXiv:astro-ph/9609066 \[astro-ph\]](#).
- [101] S. McGaugh, “Milky Way Mass Models and MOND,” *Astrophys. J.* **683** (2008) 137–148, [arXiv:0804.1314 \[astro-ph\]](#).
- [102] **Fermi-LAT** Collaboration, M. Ackermann *et al.*, “Observations of M31 and M33 with the Fermi Large Area Telescope: A Galactic Center Excess in Andromeda?,” *Astrophys. J.* **836** no. 2, (2017) 208, [arXiv:1702.08602 \[astro-ph.HE\]](#).
- [103] A. Geringer-Sameth, M. G. Walker, S. M. Koushiappas, S. E. Kuposov, V. Belokurov, G. Torrealba, and N. W. Evans, “Indication of Gamma-ray Emission from the Newly Discovered Dwarf Galaxy Reticulum II,” *Phys. Rev. Lett.* **115** no. 8, (2015) 081101, [arXiv:1503.02320 \[astro-ph.HE\]](#).
- [104] V. Bonnavard, C. Combet, D. Maurin, A. Geringer-Sameth, S. M. Koushiappas, M. G. Walker, M. Mateo, E. W. Olszewski, and J. I. Bailey III, “Dark matter annihilation and decay profiles for the Reticulum II dwarf spheroidal galaxy,” *Astrophys. J.* **808** no. 2, (2015) L36, [arXiv:1504.03309 \[astro-ph.HE\]](#).
- [105] **DES**, **Fermi-LAT** Collaboration, A. Albert *et al.*, “Searching for Dark Matter Annihilation in

- Recently Discovered Milky Way Satellites with Fermi-LAT,” *Astrophys. J.* **834** no. 2, (2017) 110, [arXiv:1611.03184 \[astro-ph.HE\]](#).
- [106] A. Alves, S. Profumo, F. S. Queiroz, and W. Shepherd, “Effective field theory approach to the Galactic Center gamma-ray excess,” *Phys. Rev.* **D90** no. 11, (2014) 115003, [arXiv:1403.5027 \[hep-ph\]](#).
- [107] P. Agrawal, M. Blanke, and K. Gemmler, “Flavored dark matter beyond Minimal Flavor Violation,” *JHEP* **10** (2014) 72, [arXiv:1405.6709 \[hep-ph\]](#).
- [108] S. Ipek, D. McKeen, and A. E. Nelson, “A Renormalizable Model for the Galactic Center Gamma Ray Excess from Dark Matter Annihilation,” *Phys. Rev.* **D90** no. 5, (2014) 055021, [arXiv:1404.3716 \[hep-ph\]](#).
- [109] C. Boehm, M. J. Dolan, and C. McCabe, “A weighty interpretation of the Galactic Centre excess,” *Phys. Rev.* **D90** no. 2, (2014) 023531, [arXiv:1404.4977 \[hep-ph\]](#).
- [110] M. Abdullah, A. DiFranzo, A. Rajaraman, T. M. P. Tait, P. Tanedo, and A. M. Wijangco, “Hidden on-shell mediators for the Galactic Center γ -ray excess,” *Phys. Rev.* **D90** (2014) 035004, [arXiv:1404.6528 \[hep-ph\]](#).
- [111] A. Martin, J. Shelton, and J. Unwin, “Fitting the Galactic Center Gamma-Ray Excess with Cascade Annihilations,” *Phys. Rev.* **D90** no. 10, (2014) 103513, [arXiv:1405.0272 \[hep-ph\]](#).
- [112] N. F. Bell, S. Horiuchi, and I. M. Shoemaker, “Annihilating Asymmetric Dark Matter,” *Phys. Rev.* **D91** no. 2, (2015) 023505, [arXiv:1408.5142 \[hep-ph\]](#).
- [113] M. Freytsis, D. J. Robinson, and Y. Tsai, “Galactic Center Gamma-Ray Excess through a Dark Shower,” *Phys. Rev.* **D91** no. 3, (2015) 035028, [arXiv:1410.3818 \[hep-ph\]](#).
- [114] P. Agrawal, B. Batell, P. J. Fox, and R. Harnik, “WIMPs at the Galactic Center,” *JCAP* **1505** (2015) 011, [arXiv:1411.2592 \[hep-ph\]](#).
- [115] M. R. Buckley, D. Feld, and D. Goncalves, “Scalar Simplified Models for Dark Matter,” *Phys. Rev.* **D91** (2015) 015017, [arXiv:1410.6497 \[hep-ph\]](#).
- [116] G. Elor, N. L. Rodd, and T. R. Slatyer, “Multistep cascade annihilations of dark matter and the Galactic Center excess,” *Phys. Rev.* **D91** (2015) 103531, [arXiv:1503.01773 \[hep-ph\]](#).
- [117] M. Kaplinghat, T. Linden, and H.-B. Yu, “Galactic Center Excess in γ Rays from Annihilation of Self-Interacting Dark Matter,” *Phys. Rev. Lett.* **114** no. 21, (2015) 211303, [arXiv:1501.03507 \[hep-ph\]](#).
- [118] C. Karwin, S. Murgia, T. M. P. Tait, T. A. Porter, and P. Tanedo, “Dark Matter Interpretation of the Fermi-LAT Observation Toward the Galactic Center,” *Phys. Rev.* **D95** no. 10, (2017) 103005, [arXiv:1612.05687 \[hep-ph\]](#).
- [119] H. A. Clark, P. Scott, R. Trotta, and G. F. Lewis, “Substructure considerations rule out dark matter interpretation of Fermi Galactic Center excess,” [arXiv:1612.01539 \[astro-ph.HE\]](#).
- [120] G. Elor, N. L. Rodd, T. R. Slatyer, and W. Xue, “Model-Independent Indirect Detection Constraints on Hidden Sector Dark Matter,” *JCAP* **1606** no. 06, (2016) 024, [arXiv:1511.08787 \[hep-ph\]](#).
- [121] T. Sjostrand, S. Mrenna, and P. Z. Skands, “PYTHIA 6.4 Physics and Manual,” *JHEP* **05** (2006) 026, [arXiv:hep-ph/0603175 \[hep-ph\]](#).
- [122] T. Sjostrand, S. Mrenna, and P. Z. Skands, “A Brief Introduction to PYTHIA 8.1,” *Comput. Phys. Commun.* **178** (2008) 852–867, [arXiv:0710.3820 \[hep-ph\]](#).
- [123] M. Cirelli, G. Corcella, A. Hektor, G. Hutsi, M. Kadastik, P. Panci, M. Raidal, F. Sala, and

- A. Strumia, “PPPC 4 DM ID: A Poor Particle Physicist Cookbook for Dark Matter Indirect Detection,” *JCAP* **1103** (2011) 051, [arXiv:1012.4515 \[hep-ph\]](#). [Erratum: JCAP1210,E01(2012)].
- [124] P. Ciafaloni, D. Comelli, A. Riotto, F. Sala, A. Strumia, and A. Urbano, “Weak Corrections are Relevant for Dark Matter Indirect Detection,” *JCAP* **1103** (2011) 019, [arXiv:1009.0224 \[hep-ph\]](#).
- [125] F. Calore, M. Di Mauro, F. Donato, J. W. T. Hessels, and C. Weniger, “Radio detection prospects for a bulge population of millisecond pulsars as suggested by Fermi LAT observations of the inner Galaxy,” *Astrophys. J.* **827** no. 2, (2016) 143, [arXiv:1512.06825 \[astro-ph.HE\]](#).